Structural Basis of the Ferrous Iron Specificity of the Yeast Ferroxidase, Fet3p[†]

Christopher S. Stoj,[‡,§] Anthony J. Augustine,[||] Lynn Zeigler,[‡] Edward I. Solomon,[||] and Daniel J. Kosman*[,‡]

Department of Biochemistry, School of Medicine and Biological Sciences, State University of New York, Buffalo, New York 14214, and Department of Chemistry, Stanford University, Stanford, California 94305

Received July 31, 2006; Revised Manuscript Received September 1, 2006

ABSTRACT: Fet3p is a multicopper oxidase (MCO) that functions together with the iron permease, Ftr1p, to support high-affinity Fe uptake in yeast. Fet3p is a ferroxidase that, like ceruloplasmin and hephaestin, couples the oxidation of 4 equiv of Fe^{II} to the reduction of O_2 to $2H_2O$. The ferrous iron specificity of this subclass of MCO proteins has not been delineated by rigorous structure−function analysis. Here the crystal structure of Fet3p has been used as a template to identify the amino acid residues that confer this substrate specificity and then to quantify the contributions they make to this specific reactivity by thermodynamic and kinetic analyses. In terms of the Marcus theory of outer-sphere electron transfer, we show here that D283, E185, and D409 in Fet3p provide a Fe^{II} binding site that actually favors ferric iron; this site thus reduces the reduction potential of the bound Fe^{II} in comparison to that of aqueous ferrous iron, providing a thermodynamically more robust driving force for electron transfer. In addition, E185 and D409 constitute parts of the electron-transfer pathway from the bound Fe^{II} to the protein's type 1 Cu^{II}. This electronic matrix coupling relies on H-bonds from the carboxylate OD2 atom of each residue to the NE2 NH group of the two histidine ligands at the type 1 Cu site. These two acidic residues and this H-bond network appear to distinguish a fungal ferroxidase from a fungal laccase since the specificity that Fet3p has for Fe^{II} is completely lost in a Fet3pE185A/D409A mutant. Indeed, this double mutant functions kinetically better as a laccase, albeit a relatively inefficient one.

Multicopper oxidases (MCOs)[1] are distinguished because they contain at least four copper atoms and the three types of Cu sites found in nature, copper site types 1, 2, and 3. In all of the MCOs, these copper sites are positioned using a series of structurally conserved Greek-key, β-barrel cupredoxin domains. The Pfam web site (Sanger Institute) lists more than 1200 candidate MCO proteins distributed among all three domains which couple the oxidation of 4 equiv of a one-electron reductant to the four-electron reduction of dioxygen, O_2, to $2H_2O$ (*1*, *2*).

Aromatic phenols and amines like hydroquinone (HQ) and *p*-phenylenediamine are substrates common to all MCOs. This substrate reactivity supports the likely physiologic functions of the laccases in wound healing in plants and pigmentation in fungi. However, among MCOs, there is a subclass of enzymes that exhibit specificity toward low-valent transition metals, e.g., Fe^{II}, Cu^{I}, and Mn^{II}, in comparison to HQ, for example. On the basis of this unique reactivity, these MCOs have been described as metallooxidases (*2*, *3*).

The most thoroughly characterized of these metallooxidases are the ferroxidases, MCOs that have high reactivity toward Fe^{II} as a reducing substrate (*4*). These enzymes are widely distributed in yeasts, blue-green algae, and mammals; also, paralogs are common in many species (*2*). For example, mammals produce both ceruloplasmin (Cp) (*5*, *6*), a soluble ferroxidase found in plasma and interstitial fluid, and hephaestin (Hp) (*7*, *8*). The paralogs in *Saccharomyces cerevisiae* are the Fet3 (*9*, *10*) and Fet5 (*11*) proteins.

As noted, these MCOs use ferrous iron as their physiological substrate and thus catalyze the ferroxidase reaction shown in eq 1.

$$4Fe^{II} + O_2 + 4H^+ \rightarrow 4Fe^{III} + 2H_2O \qquad (1)$$

The ferroxidase activity these enzymes share is critical to normal iron homeostasis in their respective organisms. Cp aids in the trafficking of iron from intestinal epithelial cells to transferrin and in clearing Fe^{II} from the interstities of the brain (*5*, *12*), while Hp is involved in the release of iron at the basolateral membrane of enterocytes into the bloodstream (*8*). Fet3p, together with the ferric permease, Ftr1p, is required for high-affinity iron uptake (*13*); Fet5p and Fth1p together support efflux of Fe from the yeast vacuole (*11*).

Several investigators have attempted to probe the nature of the iron binding site within Fet3p. In particular, the Solomon and Kosman labs have focused on the rate of electron transfer from the reducing substrate to the T1 Cu^{II} in Fet3p and hCp as well as on steady-state dioxygen

[†] This work was supported by National Institutes of Health Grant DK53820 (D.J.K.) and Grant DK31450 (E.I.S.) from the U.S. Public Health Service.

* To whom correspondence should be addressed. Phone: (716) 829-2842. Fax: (716) 829-2661. E-mail: camkos@buffalo.edu.

[‡] State University of New York.

[§] Current address: Department of Biochemistry, Chemistry and Physics, Niagara University, Niagara Falls, NY 14109.

[||] Stanford University.

[1] Abbreviations: MCO, multicopper oxidase; HQ, hydroquinone; Cp, ceruloplasmin; Hp, hephaestin; TM, transmembrane (domain); *Cc* Lc, *Coprinus cinereus* laccase; VTVH MCD, variable-temperature, variable-field magnetic circular dichroism; MES, 2-(*N*-morpholino)ethanesulfonic acid; ET, electron transfer; GFP, green fluorescent protein.

10.1021/bi061543+ CCC: $33.50
Published on Web 10/03/2006

reduction kinetics (*14*, *15*). In the former studies, the rates of reduction of the T1 Cu^{II} under single-turnover conditions by HQ and by Fe^{II} in Fet3p and hCp were compared to these rates in *Coprinus cinereus* laccase (*Cc* Lc). With a reduction potential of 70 mV, HQ is a better reductant than Fe^{II} by ~350 mV at pH 6.0; also, with a reduction potential of 550 mV (*16*), the T1 Cu^{II} in *Cc* Lc is a better oxidant than the T1 Cu^{II} in Fet3p (E° = 427 mV) (*17*) or the two redox-active T1 sites in hCp (448 mV) (*18*). Despite the large difference in driving force for electron transfer from HQ in comparison to that of Fe^{II} to the T1 Cu^{II} in Fet3p, reduction of Fet3p by Fe^{II} was at least 5-fold faster than reduction by HQ. Furthermore, reduction of the T1 Cu^{II} in Fet3p by Fe^{II} was >65-fold faster than reduction of the T1 Cu^{II} in *Cc* Lc despite the latter's ~120 mV advantage in oxidation potential. A last thermodynamically significant aspect of the hCp and Fet3p single-turnover electron-transfer reactions with both reductants was that complete reduction of all four protein Cu^{II} atoms (five in the case of hCp) was achieved with as few as 7 electron equivalents of reductant (*17*, *18*). While for HQ this is reasonable given the ~400 mV equilibrium driving force, this near-stoichiometric redox reaction with Fe^{II} as a reductant is at odds with this species E°; as noted, this value is not different from the E° for the T1 Cu^{II} sites in either Fet3p or hCp. These are the kinetic and thermodynamic characteristics of the intermolecular electron-transfer reactions that separate the ferroxidases from the rest of the MCO protein family.

The crystal structure of the soluble exocytoplasmic MCO domain of Fet3p (*19*) allows us now to delineate the structural origins of these reactivity differences. On the basis of this structure, we have targeted specific residues at the T1 Cu^{II} site of this protein and quantified the contribution that each makes to the intermolecular electron transfer at this site. The results described herein provide strong evidence that the iron binding site in Fet3p is comprised of residues E185, D409, and D283. Our kinetic analyses provide specific information about how each contributes to Fe^{II} binding, to intermolecular electron transfer, and to trafficking of Fe^{III} to Ftr1p. This work makes clear the structural differences between a laccase and ferroxidase that confer the metallooxidase specificity to this specialized member of the MCO protein family.

MATERIALS AND METHODS

Expression and Purification of Soluble Fet3. S. cerevisiae strain M2* carrying plasmid pDY148 was used as the expression system for the purification of soluble Fet3p (*10*). This strain is *MAT*α *trp1-63 leu2*-3,112 gcn4-101 his3-609 ura3-52 AFT1-1^{up}. The *AFT1-*1^{up} allele encodes a dominant, gain-of-function mutant of the Aft1 protein, the transactivator of the genes of the iron regulon, including *FET3*. Plasmid pDY148 is a high-copy vector that carries a recombinant *FET3* effectively truncated at nucleotide 1666 (at amino acid residue 555). This truncation removed the apparent membrane-spanning domain found in the carboxy-terminal region that is included in residues 559−586. Expression of Fet3p from pDY148 results in a Fet3p with a carboxy-terminal FLAG tag that was secreted directly into the growth medium rather than being retained in the plasma membrane. Fet3 protein production and purification have been described previously in some detail (*10*).

Construction of Fet3p Mutants. Mutant *FET3* alleles were constructed directly in pDY148 (for secreted, soluble Fet3p) and in pDY133 (for the native membrane-associated Fet3p) by site-directed mutagenesis using the QuikChange kit from Stratagene. Briefly, complementary primers were used in PCR amplification of the appropriate vector to generate Fet3pE185A, -D283A, and -D409A single mutants and then in two sequential rounds of mutagenesis to produce the Fet3pE185A/D409A double mutant. Mutated *FET3* sequences were confirmed by automated fluorescence sequencing on an ABI PRISM 377 instrument. Vectors expressing the mutant proteins were transformed into yeast strain M2* for soluble protein expression (*10*) and in strain AJS05 for in vivo analyses of protein localization at the plasma membrane and ^{59}Fe uptake (*20*).

Protein Characterization. Room-temperature UV−visible absorption spectra were recorded using a Varian Cary 50 spectrophotometer. The protein concentration was determined using the standard dye binding Bradford assay using BSA as the protein standard (*21*). The copper content of each enzyme was determined by absorbance at 546 nm using the biquinoline reagent (0.5 mg/mL 2,2-biquinoline in glacial acetic acid) compared to $CuSO_4$ standards prepared in 100 mM imidazole/acetate buffer at pH 6.5 (*22*). EPR spectra were obtained using a Bruker EMX spectrometer, an ER 041 XG microwave bridge, and an ER 4102ST cavity; samples were tested at 77 K. Reduction potentials of the T1 Cu were obtained by the poised potential method (*17*). A 200 μL sample of ~0.1 mM degassed protein in 100 mM phosphate buffer at pH 6.5 was placed in a 1 cm path length anaerobic cuvette with a Teflon septum, and degassed $K_3[Fe(CN)_6]$ was added to yield a final concentration of ~5 mM. Aliquots of degassed $K_4[Fe(CN)_6]$ were added, and absorption at 608 nm was monitored at room temperature over time until equilibrium was achieved for each titration point (15−20 min). The absorbance versus potential data were fit to the Nernst equation using Prism 4 from GraphPad (San Diego, CA).

Steady-State Turnover Kinetic Analysis. All O_2 uptake analyses were based on oxygen consumption using an Oxygraph (Hansatech, www.hansatech-instruments.co.uk). Rates of O_2 uptake were evaluated using the OXYG32 software provided by Hansatech. All initial velocity, v, versus [S] data were subsequently analyzed by direct fitting to the Michaelis−Menten equation using Prism 4. Ferrous ammonium sulfate and hydroquinone (HQ) were used for kinetic analysis of the ferroxidase and oxidase activity of Fet3 proteins, respectively. Stock solutions of the substrates were freshly prepared in nitrogen-purged 100 mM MES at pH 6.0. All transfers from these stock solutions were carried out using gastight syringes. The buffer used for O_2 uptake measurements was air-saturated 100 mM MES at pH 6.0.

Type 1 Cu Single-Turnover Kinetic Analyses. T1 Cu^{II} reduction rates were obtained using an Applied Photophysics SX.18MV stopped-flow absorption spectrophotometer equipped with a Hg/Xe Arc lamp and outfitted with PEEK tubing; the dead time of the instrument was ~2 ms. The stopped-flow kinetic experiments were performed at 4 °C in 100 mM phosphate buffer (pH 6.5), with a final protein concentration of ~50 μM; reduction of the four Cu^{II} atoms in Fet3p was followed by the T1 Cu^{II} absorbance at 608 nm with a cell path length of 1 cm. The tubing, plungers, and

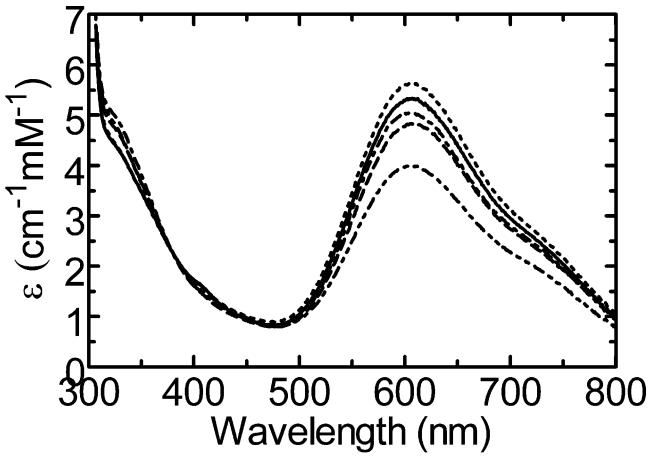

FIGURE 1: Absorption spectra of wild-type and mutant Fet3 proteins. Room-temperature UV−vis absorbance spectra of the wild type (—), E185A (− − −), D283A (- - -), D409A (− - −), and E185A/D409A (− - - −). Absorbance is given as the millimolar extinction coefficient calculated from spectra normalized for protein concentration.

valves were rendered anaerobic when they were washed with a dithionite solution followed by several washes with degassed water or buffer; the system was operated under a positive pressure of N_2 to maintain anaerobiosis. A minimum of three reduction−absorbance traces for a given reaction were subsequently fit to equations describing single- or parallel first-order reactions using Prism 4.

RESULTS

Characterization of Fet3p Mutants. Fet3p mutants E185A, D283A, D409A, and E185A/D409A were expressed in yeast as soluble, secreted proteins as a result of the carboxy-terminal truncation of their transmembrane domain as described previously (*10*). The UV−vis absorption spectra of Fet3p have been shown to contain two dominant features: the intense absorbance at 608 nm (ϵ = 5500 M^{-1} cm^{-1}) as a result of significant S → Cu charge transfer from C484, a ligand to the T1 Cu, and a shoulder at 330 nm (ϵ = 5000 M^{-1} cm^{-1}) assigned as a charge transfer from the bridging OH group to the two T3 Cu^{II} atoms. These spectra for the protein samples used in this study showed only minor variation in their absorptivities with the exception of the E185A/D409A protein; this Fet3p mutant consistently exhibited an extinction coefficient at 608 nm that was ∼25% less than that of the wild type while exhibiting normal absorbance at 330 nm (Figure 1). This decreased T1 Cu^{II} absorbance was not the result of incomplete copper loading, as all proteins were purified with four copper atoms per Fet3p molecule (Table 1). The X-band cwEPR spectra for all four mutant proteins were comparable to that of the wild type, suggesting that any changes in the electronic and geometric features of the T1 Cu site in Fet3pE185A/D409A were too subtle to be detected by cwEPR at this level of resolution (see Figure S1 of the Supporting Information).

The Fet3pE185A and Fet3pD283A single mutants had wild-type reduction potentials (Table 1 and Figure 2). In contrast, the single and double Fet3p mutants containing the D409A mutation exhibited a dramatic ∼120 mV increase in reduction potential. Alteration of the ligand field has been shown to significantly modulate the reduction potential of

Table 1: Redox Potential, Copper Content, and Molar Absorptivity[a]

Fet3p species	T1 Cu redox potential (mV)	Cu (mol)	ϵ_{608} (cm^{-1} M^{-1})
wild type	433	4.4	5320
D283A	439	4.0	5638
E185A	433	4.1	4835
D409A	550	4.0	5039
E185A/D409A	549	4.2	3994

[a] Redox potentials were determined using the poised-potential method with the potassium ferri/ferrocyanide couple (data in Figure 2). Copper content was determined by the biquinoline method. Cu stoichiometry and extinction coefficients were calculated on the basis of the protein concentration determined using the Bradford dye binding assay.

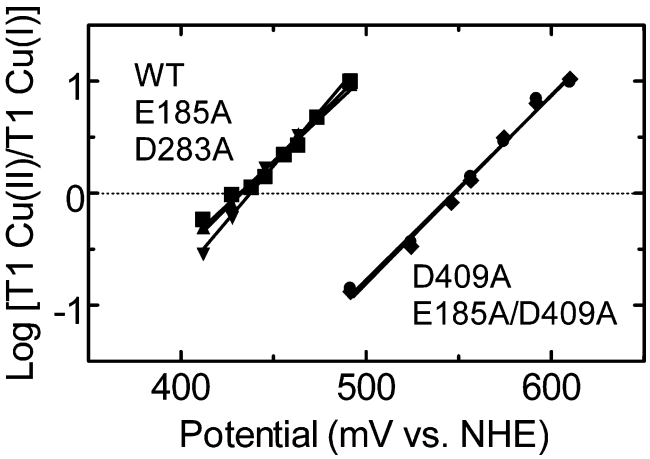

FIGURE 2: Poised potential titrations of wild-type and mutant Fet3 proteins. The solid lines are the best fits to the Nernst equation for the wild type (■), E185A (▲), D283A (▼), D409A (◆), and E185A/D409A (●). The solution potential was set by the ferri/ferrocyanide ratio.

T1 Cu sites; for example, changes in redox potential correlate with the presence or absence of an axial methionine ligand with variations in $E°$ of more than 100 mV (*23*, *24*). The data here indicate that the redox potential of the T1 Cu^{II} in Fet3p also can be strongly influenced by second-sphere amino acid residues; as discussed below, D409A is likely hydrogen-bonded to H413, one of the two His ligands at the Fet3p T1 Cu site.

Kinetic Analyses of Steady-State O_2 Uptake. The goal of this study was to identify amino acid residues within Fet3p that contribute to the coordination of ferrous iron. We therefore obtained steady-state velocity versus [S] data. These data were fit directly to the Michaelis−Menten equation, thus providing K_M values which were taken as a measure of productive substrate binding. The O_2 uptake velocities using Fe^{II} as a substrate are shown in Figure 3; the lines are the theoretical fits based on the kinetic constants given in Table 2. With Fe^{II}, wild-type Fet3p and E185A had K_M values comparable to those reported in the literature, 4.9 and 35.6 μM, respectively (*10*, *15*). Fet3p mutants D283A and D409A exhibited modest ∼4-fold increases in K_M for Fe^{II}. The double mutant E185A/D409A displayed a synergistic, ∼800-fold increase in K_M for Fe^{II}, indicating a cooperative role for at least E185 and D409 in kinetically productive Fe^{II} binding.

HQ was used as a control to show that any observed K_M changes were seen only with ferrous iron as the substrate; the data showed this to be the case (Figure 4, fitted values

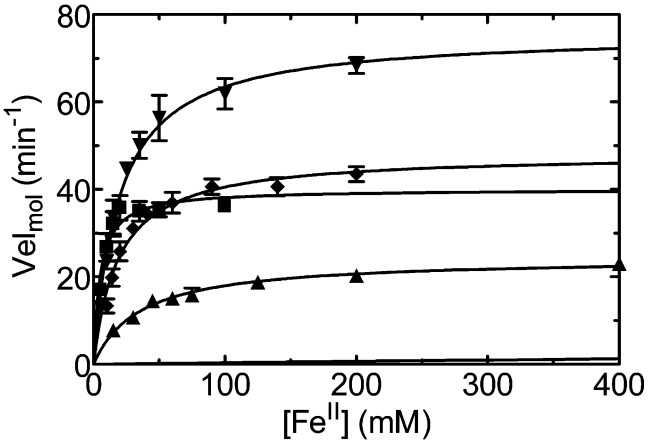

FIGURE 3: Kinetic analysis of Fe^{II} turnover by wild-type and mutant Fet3 proteins. O_2 uptake data were obtained as a function of Fe^{II} concentration using an Oxygraph oxygen electrode and the associated OXYGRAPH software. The uptake data, given as molecular velocities, for the wild type (■), E185A (▲), D283A (▼), D409A (◆), and E185A/D409A (●), were fit directly to the Michaelis−Menten equation generating the traces shown. The data points represent the average of three replicates at each iron concentration with error bars representing the standard error of the mean.

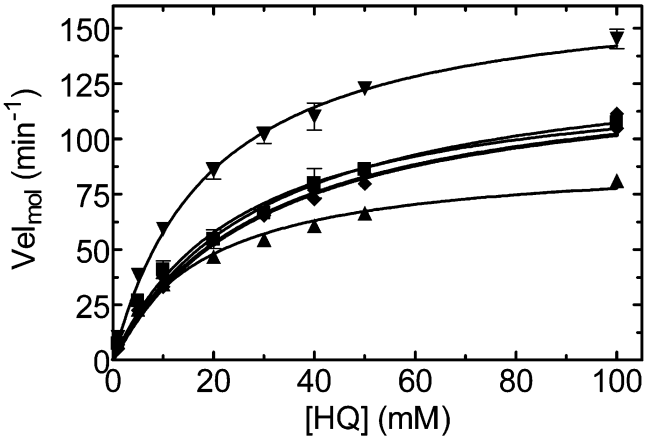

FIGURE 4: Kinetic analysis of HQ turnover by wild-type and mutant Fet3p proteins. O_2 uptake data were obtained as a function of HQ concentration using an Oxygraph oxygen electrode system and the associated OXYGRAPH software. The uptake data, given as molecular velocities, for the wild type (■), E185A (▲), D283A (▼), D409A (◆), and E185A/D409A (●) were fit directly to the Michaelis−Menten equation generating the traces shown. The data points represent the average of three replicates at each iron concentration with error bars representing the standard error of the mean.

Table 2: Steady-State Kinetic Constants and Single-Turnover Reduction Rates with Fe^{II} [a]

	steady-state Fe^{II} turnover		single-turnover reduction by Fe^{II} (s^{-1})	
Fet3p species	K_M (μM)	k_{cat} (min^{-1})	fast phase	slow phase
wild type	4.9 ± 0.8	40.1 ± 1.4	≥1500	NA[b]
D283A	19.3 ± 1.5	75.7 ± 1.9	681.9 ± 23.7	2.46 ± 0.28
E185A	35.6 ± 2.8	24.3 ± 0.6	2.47 ± 0.04	0.36 ± 0.01
D409A	18.8 ± 1.6	48.2 ± 1.2	62.03 ± 0.60	1.31 ± 0.07
E185A/D409A	3994 ± 387	13.9 ± 0.4	0.41 ± 0.01	0.02 ± 0.07

[a] Values for steady-state kinetic constants were obtained using fits to the Michaelis−Menten equation of the data shown in Figure 3. Stopped-flow T1 Cu^{II} reduction data as in Figure 5 were fit using a double-exponential nonlinear regression analysis. The lower limit for the reduction rate for the wild-type enzyme was estimated as reduction was complete within the 2 ms dead time of the instrument. [b] Not available.

Table 3: Steady-State Kinetic Constants and Single-Turnover Reduction Rates with HQ[a]

	steady-state HQ turnover		single-turnover reduction by HQ (s^{-1})	
Fet3p species	K_M (mM)	k_{cat} (min^{-1})	fast phase	slow phase
wild type	25.5 ± 2.5	131.3 ± 5.0	0.025 ± 0.000	NA[b]
D283A	19.3 ± 1.1	169.5 ± 3.5	0.072 ± 0.018	0.001 ± 0.101
E185A	18.2 ± 1.5	91.7 ± 2.6	0.102 ± 0.011	0.003 ± 0.020
D409A	30.3 ± 2.4	139.7 ± 4.7	1.124 ± 0.103	0.105 ± 0.003
E185A/D409A	30.5 ± 2.1	132.8 ± 3.9	2.127 ± 0.085	0.256 ± 0.020

[a] Values for steady-state kinetic constants were obtained using fits to the Michaelis−Menten equation of the data shown in Figure 4. Stopped-flow T1 Cu^{II} reduction data as in Figure 6 were fit using a double-exponential nonlinear regression analysis for all mutant proteins. Wild-type reduction data were fit using a single-exponential nonlinear regression model. [b] Not available.

in Table 3). There were changes in k_{cat} for turnover with both substrates, however (Tables 2 and 3). Mutation at the reducing substrate binding site would not be expected to alter the turnover k_{cat} since electron transfer from the reductant is not rate-limiting in the MCO reaction (*25*, *26*). Given the lack of a strong correlation between mutational effects on Fe^{II} versus HQ turnover (k_{cat}) and the relatively small fold differences overall, we did not examine the origin of these variations further.

Kinetic Analyses of T1 Cu^{II} Reduction Rates. Our previous studies have demonstrated that E185 plays multiple roles in both in vitro and in vivo oxidation of ferrous iron by Fet3p (*14*, *15*). Having observed altered K_M values for Fe^{II} in Fet3pD283A, -D409A, and -E185A/D4090A, we quantified the rate of intermolecular electron transfer to the T1 Cu^{II} in these mutants by stopped-flow analysis. The kinetic traces for the reduction by Fe^{II} of the oxidized enzyme's four Cu^{II} atoms monitored by the reduction of the T1 Cu^{II} are shown in Figure 5. As reported, reduction of the T1 Cu^{II} in wild-type Fet3p is very fast [$k \geq 1500$ s^{-1} (*14*)]. Mutation of E185 to alanine drastically slows the electron-transfer process, indicating E185 is a major contributor to efficient outer-sphere electron transfer to the T1 Cu. Both single mutants, D283A and D409A, exhibited decreased electron-transfer rates, also (Table 2). Fet3pE185A/D409A displayed an ~3600-fold decrease in the reduction rate, indicating that E185 and D409 function cooperatively in the electron-transfer process from bound Fe^{II} to the T1 Cu^{II}.

In comparison to fungal laccases (*25*), wild-type Fet3p exhibits very slow T1 Cu^{II} reduction rates in the presence of HQ (Figure 6). Fet3p mutants E185A and D283A exhibited reduction rates with HQ that were 3−4-fold larger than that for the wild type, while these rates for Fet3pD409A and -E185A/D409A were 45- and 85-fold larger, respectively (Table 3). These latter two ET rates reasonably are related to the significant increase in the T1 Cu^{II} redox potential for Fet3pD409A and -E185A/D409A. However, this phenotype is exactly the opposite of what we observed for ferrous iron reduction of the T1 Cu^{II} site in these mutants, which became slower when D409 (or E185) was mutated. This difference can be attributed to a direct perturbation of the electron-transfer route by which ferrous iron, but not HQ, reduces the T1 Cu^{II}. Thus, the increase in inherent driving force provided by the increased redox potential in D409A-

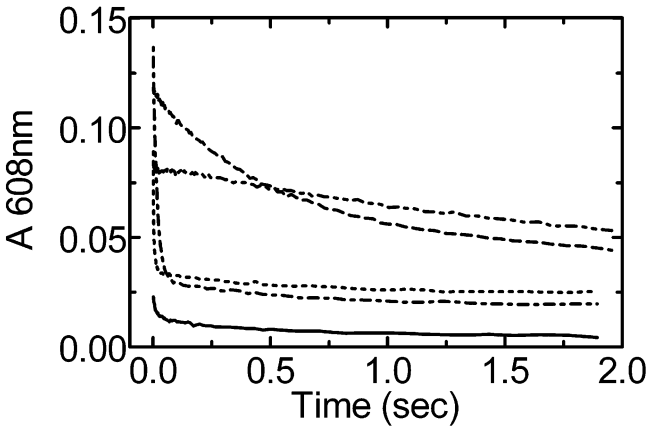

FIGURE 5: Single-turnover reduction of Fet3p Cu^{II} sites by Fe^{II}. Stopped-flow absorbance data for the wild type (—), E185A (— — —), D283A (- - -), D409A (— - —), and E185A/D409A (— - - —) by 8 equiv of Fe^{II} at 4 °C. The initial 608 nm absorbance ($t = 0$) was ~0.13. Each curve represents the average of at least three independent reactions.

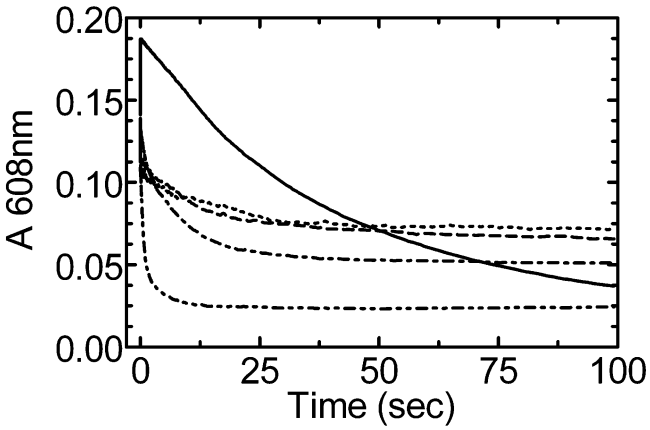

FIGURE 6: Single-turnover reduction of Fet3p Cu^{II} sites by HQ. Stopped-flow absorbance data for the wild type (—), E185A (— — —), D283A (- - -), D409A (— - —), and E185A/D409A (— - - —) by 4.3 mM HQ at 4 °C. The initial 608 nm absorbance ($t = 0$) was ~0.19. Each curve represents the average of at least three independent reactions.

containing mutants appears to be offset, in the case of Fe^{II} as the substrate, by the elimination of an electron-transfer pathway linking the bound iron to the T1 Cu^{II} site, a pathway apparently not employed by HQ. Data for T1 Cu^{II} reduction in Fet3p consistently fit better to a double-exponential first-order equation irrespective of reducing substrate (cf. Tables 2 and 3, last columns); the amplitude of the slow process is typically <20% of the total. We have not been able to elucidate the origin of this kinetic phenomenon (*14*, *17*).

Kinetic Analysis of ^{59}Fe Uptake. To assess the cellular significance of these defects in Fe^{II} reactivity with Fet3p mutants, ^{59}Fe uptake assays were performed in cells expressing wild-type or mutant forms of the native, membrane-bound form of the protein in complex with the permease, Ftr1p. Our standard uptake buffer includes 20 mM citrate (*27*); in this buffer, all of the mutants were defective in ^{59}Fe accumulation (Table S1 of the Supporting Information). The severity of the iron uptake phenotype varied among the single mutants, however, as wild-type uptake is restored in D283A and D409A when citrate is withheld from the iron uptake buffer. This was not true for mutants containing the E185A substitution; this mutation completely disabled the Fe uptake function of Fet3p irrespective of the uptake conditions. The ability of citrate to perturb iron uptake is indicative of an altered fidelity of iron channeling between Fet3p and Ftr1p as a result of these mutations (*27*). Note that none of these results can be attributed to variation in plasma membrane localization of the Fet3p−Ftr1p iron uptake complex as all mutants moved properly as indicated by the correct localization of Ftr1:GFP determined by confocal fluorescence microscopy (data not shown; see refs *15* and *27*).

DISCUSSION

Of the >1000 proteins identified as MCOs on the basis of the tripartite cuprodoxin Cu-binding motif, only a few have been demonstrated or predicted to function as ferroxidases; of this subset, only Cp and Fet3p have been kinetically characterized, and only Fet3p has been examined in some detail by protein engineering approaches. The crystal structure of hCp indicated the presence of a Fe^{II} binding site formed by residues E272, H940, E935, and D1025 between domains 2 and 6 (*28*, *29*). This crystallographic analysis provided some initial insight into the structural features of ferrous iron binding by an MCO, but the lack of significant sequence identity with Fet3p and the fact that Cp contains six domains versus three for Fet3p limited the usefulness of the hCp structure as a paradigm for the iron binding site within Fet3p itself. Indeed, the use of homology modeling to identify the structural features in Fet3p that confer this unique substrate selectivity has yielded mixed results (*15*, *30*). Now, however, the crystal structure of Fet3p allows for a knowledge-based interpretation of the kinetic results provided here and in previous reports (*14*, *15*, *17*, *31*).

This structure shows that E185 is positioned near the solvent-exposed surface of Fet3p directly above the T1 Cu and via the OE2 atom forms an apparent hydrogen bond with NE2 of H489, one of the histidine ligands to the T1 Cu. The structure of Fet3p suggests a similar role for D409, hydrogen-bonded via the OD2 atom to NE2 of H413, the other histidine ligand to the T1 Cu (*19*). D409 and E185 thereby act as extensions of the T1 Cu coordination sphere associated with the two His residues. This study addresses the roles of these two complementary residues and of D283 in ferrous iron binding, electron transfer, and iron trafficking processes within Fet3p; D283 is found above and positioned between E185 and D409 and the solvent at the surface of Fet3p. This model of Fet3p and its binding of Fe^{II} is illustrated in Figure 7.

The results from our steady-state kinetic analyses demonstrate the importance of E185, D283, and D409 in kinetically productive ferrous iron binding. Fet3pE185A exhibited an ~8-fold increase in K_M for Fe^{II}; Fet3pD283A and -D409A also displayed increases in K_M with iron of ~4-fold in each case (see Table 2). The double mutant Fet3pE185A/D409A exhibited a synergistic >800-fold increase in K_M, suggesting that binding of Fe^{II} to E185 and D409 is cooperative (*32*, *33*). In contrast, all of the mutants displayed wild-type K_M values for HQ, all of which are in the low millimolar range. Thus, the alterations in productive substrate binding in these mutants are specific for Fe^{II}. In fact, both E185A and D409A mutations completely altered the ability of this mutant to discriminate between Fe^{II} and HQ; indeed, Fet3pE185A/D409A is indistinguishable from

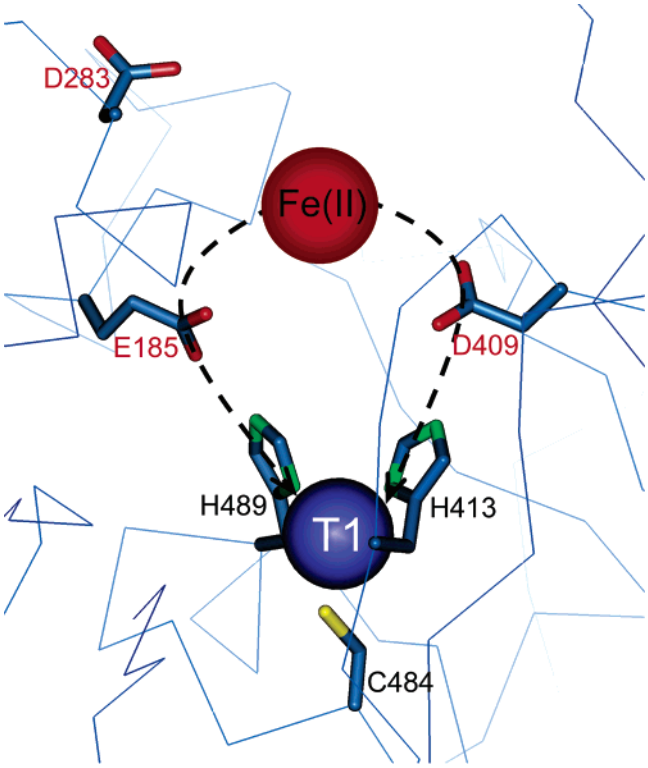

FIGURE 7: Proposed Fe^{II} binding and electron-transfer site in Fet3p. The iron binding residues E185, D283, and D409 are shown relative to the T1 Cu site. Residues that coordinate the T1 copper (blue) include H413, C484, and H489. The crystal structure indicates that the OD2 carboxylate oxygens of E185 and D409 are H-bonded to the NE2 NH groups of H489 and H413, respectively. The dashed arrows indicate the electron-transfer pathways from the Fe^{II} species to the T1 Cu as determined using PATHWAYS (*37*). The two carboxylate−imidazole H-bonds are essential components of these pathways.

a laccase with respect to substrate specificity. This reverse engineering (from the point of view of a ferroxidase) is best illustrated by k_{cat}/K_M values. For Fe^{II} and HQ, these values for wild-type Fet3p are 8.2×10^6 and 5.1×10^3 M^{-1} min^{-1}, respectively; for Fet3pE185A/D409A, these values are 3.5×10^3 and 4.4×10^3 M^{-1} min^{-1}, respectively. In other words, the ferroxidase specificity of Fet3p (by a factor of 10^3) has been completely suppressed in the double mutant.

The single-turnover, intermolecular reduction rate differences between wild-type and mutant Fet3 proteins reflect how the Marcus theory of outer-sphere electron transfer applies to the ferroxidase reaction catalyzed by any MCO and this ferrous iron substrate specificity. This theory is described by eq 2.

$$k_{ET} = SK_A\left(\frac{4\pi^3}{h^2\lambda k_B T}\right)^{1/2}(H_{DA})^2 e^{-(\Delta G^\circ+\lambda)^2/4\lambda k_B T} \qquad (2)$$

In the Marcus equation (*34*), the rate of electron transfer, k_{ET}, is governed first by the steric term, S, and the equilibrium constant for formation of the interaction complex between the electron donor and acceptor, K_A. The steric term represents that fraction of the complex that is competent for electron transfer, reflecting what the enzyme kineticist would call productive binding; thus, the product, SK_A, is equivalent to $1/K_M$, since K_M, in effect, is the effective substrate dissociation constant from a productive Michealis complex.

Table 4: Correlation between Observed and Predicted Reduction of the T1 Cu^{II} Rate by Fe^{II} [a]

	observed k_{ET} (s^{-1})	predicted k_{ET} based on individual Marcus terms (fold change due to each term) $1/K_M = SK_A$	ΔG° (E°)	H_{DA}	calcld k_{ET} (s^{-1})
wild type	≥1500				
D283A	682	375 (0.25)	NC	wild type	375
E185A	2.5	210 (0.14)	NC	165 (0.11)	22
D409A	62	390 (0.26)	18000 (12.2)	660 (0.44)	165
E185A/D409A	0.4	1.5 (0.001)	18000 (12.2)	75 (0.05)	0.08

[a] The values relate the predicted k_{ET} and fold change for the individual Marcus terms (see eq 2) relative to the observed wild-type Fet3p reduction rate with Fe^{II} as the substrate. The calculated values for k_{ET} were determined as the sum of the individual terms as per the Marcus equation. The value of H_{DA} was calculated using PATHWAYS (*37*) and the coordinates for Fet3p (PDB entry 1ZPU).

The electronic matrix coupling element, H_{DA}, provides a measure of the relative conductivity of the combination of through-bond and through-space jumps the electron must navigate in its path from donor to acceptor molecular orbital. The thermodynamic driving force for this electron transfer is given by ΔG°, related to the difference in reduction potentials of the donor and acceptor by the Nernst equation; for a one-electron transfer process, as in the MCO reaction, a 60 mV difference in potential is equivalent to a ΔG° of approximately −5.8 kJ/mol. Last, the reorganization energy, λ, is the energy required to change the geometry of the T1 Cu with a change in redox state, from Cu(II) to Cu(I). This value has not been measured in any MCO, but changes in this value for the T1 Cu sites in the parental mononuclear blue copper protein family have been estimated (*35*); at the extreme, these estimates indicate that at most a change in λ might contribute a a change in k_{ET} of a factor of 2-fold. Here, the absorption spectra, redox potentials, and EPR spectra indicate that the T1 Cu site is not strongly perturbed upon mutation of either E185 or D283. Therefore, the reorganization energy is likely unchanged in these mutants. However, λ may be altered in the two Fet3p mutants containing the D409A mutation. Although the absorption and EPR spectra of these mutants are similar to those of wild-type Fet3p, the large increase in redox potential observed could reflect a decrease in the reorganization energy. Correlations of this type have been reported in mononuclear blue copper proteins (*36*).

Our steady-state and single-turnover kinetic analyses provide the means to estimate the contribution to each of the terms in the Marcus equation made by each of the three Fe^{II}-binding ligands examined here. The role of D283 in outer-sphere electron transfer from Fe^{II} is the most straightforward. Due to the location of D283 and its lack of interaction with the residues coordinating the T1 Cu (Figure 7), and the normal redox potential, absorption, and EPR spectra exhibited by Fet3pD283A, we anticipated that this mutation would not significantly alter k_{ET}. Indeed, this substitution at residue D283 resulted in a minor ~2-fold reduction in k_{ET} with Fe^{II} as the reductant. This change in the ET rate can be attributed solely to the ~4-fold increase in K_M for Fe^{II} in steady-state turnover, equivalent to the $1/SK_A$ term in the Marcus equation. This analysis is summarized in line 2 of Table 4. In other words, D283 contributes to the ferroxidase specificity of Fet3p by contributing to the

productive binding of Fe^{II} for intermolecular electron transfer; this residue does not appear to contribute to the electronic coupling of the donor and acceptor or to their potential differences that provide the driving force.

In comparison to D283, E185 plays a significantly greater role in electron transfer from Fe^{II} to the T1 Cu; mutation of E185 to alanine results in ~600-fold reduction in k_{ET} from this reductant. The Marcus equation predicts that the 8-fold increase in K_M for Fe^{II} can account for only 1−2% of this reduction (Table 4, line 3). Also, Fet3pE185A exhibited wild-type absorption and EPR spectra, suggesting that λ was unaltered by this substitution, and a normal T1 Cu redox potential that would suggest a similar driving force. Therefore, a significant alteration in the electronic matrix coupling (H_{DA}) between the enzyme-bound Fe^{II} and the T1 Cu^{II} site must occur upon mutation of E185. The crystal structure of Fet3p allows for an estimation of H_{DA} into the T1 Cu^{II} via the E185−H489 pathway (Figure 7). The efficiency of this coupling was calculated by using PATHWAYS which estimates the probability of electron transfer through covalent bonds, hydrogen bonds, and space jumps to identify viable electron-transfer pathways between the donor and acceptor in an outer-sphere electron-transfer process (*37*). The analysis predicted a decay coupling for this route of 0.024. For comparison, the primary electron-transfer pathway into Cp from Fe^{II} is characterized by a decay coupling of 0.028 (*14*). Mutation of E185 to alanine would effectively eliminate this electron-transfer pathway which in the Marcus equation appears as an ~9-fold reduction in H_{DA}^2 and, therefore, an ~9-fold reduction in k_{ET} relative to that of the wild type. By multiplying the deficits in productive substrate binding (K_M) and in electronic coupling (H_{DA}) in Fet3pE185A, we find the calculated k_{ET} equals ~22 s^{-1} (Table 4). This compares to the observed k_{ET} for E185A of 2.5 s^{-1}. Our analysis apparently fails to account for an additional and quantitatively significant contribution that E185 makes to electron transfer from Fe^{II} to the Fet3p T1 Cu.

A clue to this contribution is that reduction of the T1 Cu^{II} by Fe^{II} is stoichiometric; that is, 1 equiv of Fe^{II} reduces 1 equiv of the T1 Cu^{II} in Fet3p (and 4 equiv fully reduces the protein's four prosthetic group Cu^{II} atoms). This thermodynamic behavior is inconsistent with the essentially identical reduction potentials for aqueous Fe^{II} at pH 6.5 (~420 mV) and the T1 Cu^{II} (433 mV). This similarity in reduction potential also cannot account for the driving force indicated by the fast ET rate with Fe^{II} as the reductant. These paradoxes can be resolved if we assume that the Fet3p-bound Fe^{II} has an $E°$ of ≤190 mV (*14*). Thus, Fet3p has a binding site which tunes the bound Fe^{II} for ET by providing a binding site that favors Fe^{III}. In effect, the Fet3p·Fe^{II} complex "looks like" the transition state for electron transfer. The kinetic data for the E185A mutant support this hypothesis. With respect to the 10-fold difference between the calculated and observed effects on k_{ET} summarized above for Fet3pE185A, we can now propose that E185A contributes to the required ≥240 mV reduction in the $E°$ of the bound in comparison to aqueous Fe^{II} and that this contribution is reflected in the 9-fold difference between the values of 2.5 (observed) and 22.5 s^{-1} (calculated) in Table 4 for this mutant protein.

As for Fet3pD409A, the ~4-fold decrease in the level of productive Fe^{II} binding does not correlate with the observed 24-fold reduction in k_{ET}. Furthermore, Fet3p mutants containing D409A exhibit an ~120 mV increase in redox potential which is worth ~10.5 kJ/mol to $\Delta G°$ (favorable). The Marcus equation predicts mutants containing the D409A mutation should exhibit an ~12-fold increase in k_{ET} relative to that of wild-type Fet3p due to this 120 mV increase in redox potential (Table 4, line 4). These apparent inconsistencies can be resolved first by noting that the Fet3p structure suggests that D409 is comparable to E185 in ferrous iron binding and electronic matrix coupling as shown in Figure 7. PATHWAYS predicts a decay coupling for the D409−H413 pathway of 0.012. If the change in $E°$ for Fet3pD409A is neglected, the ~2-fold reduction of H_{DA}^2 combined with the ~4-fold productive substrate binding defect predicts a calculated k_{ET} of 165 s^{-1} for this mutant, or ~3-fold larger than the observed k_{ET} of 62 s^{-1} (Table 4). That the two values are on the same order of magnitude suggests that the increase in driving force expected from the change in T1 Cu^{II} reduction potential is masked by a contribution that D409 makes to tuning the potential of the bound Fe^{II} down toward 190 mV. A change in k_{ET} due to a possible change in reorganization energy resulting from the D409A substitution was not taken into account in these calculations.

The most dramatic ET defect was seen in Fet3pE185A/D409A. The double mutant exhibited an ~3700-fold reduction in k_{ET}. By factoring in the combined effects of the individual E185A and D409A mutations, the calculated k_{ET} (0.08 s^{-1}) was comparable in magnitude to the observed k_{ET} (0.4 s^{-1}) (Table 4, last line). The results indicate that the E185−H489 and D409−H413 hydrogen bond pairs alone provide the electronic matrix coupling from bound Fe^{II} to the T1 Cu that confers the ferrous iron specificity of Fet3p in outer-sphere electron transfer. These two residues also make the major contribution to providing the Fe-binding site that favors Fe^{III} relative to Fe^{II}. The T1 site in the MCO CueO also contains a carboxylate−imidazole H-bond pair that likely provides a comparable cuprous ion binding site and electron-transfer pathway (*38*).

The kinetic data with HQ as the substrate (reductant) reflect both the Fe^{II} specificity that Fet3p has and the specific roles that D283, E185, and D409 play with regard to that specificity. First, for wild-type Fet3p, the rate of ET from HQ is ~$1/10^3$ the ET rate with Fe^{II} as the reductant. Second, all Fet3p mutants that were tested had k_{ET} values with HQ greater than that of the wild type; Fet3pD409A and Fet3pE185A/D409A had the largest increases in HQ k_{ET}, ~45- and ~85-fold, respectively. This increase can be directly attributed in part to the increased driving force for ET associated with the ~120 mV increase in the potential of the T1 Cu in Fet3 proteins with the D409A substitution. As discussed above, this expected increase in the ET rate was not realized when Fe^{II} was used as a reductant, indicating that ET from HQ likely does not utilize the electronic matrix coupling provided by E185 and D409. In fact, the increase in the ET rate with HQ, which was greater than can be explained by the change in potential alone, indicates that the substitution of two acidic residues with a nonpolar (and smaller) one enhances one or more other factors in the Marcus equation for ET from HQ. One possibility is that these substitutions expose to solvent the NE2 NH atoms of E185 and D409, providing a possible docking site for HQ. Electron transfer from a substrate like HQ to the T1 Cu in laccases is almost certainly via an H-bond between a

substrate OH or NH group and the pyrrole nitrogen of a coordinating histidine imidazole. A substrate analogue complex with this bonding pattern has been crystallographically characterized for *Trametes versicolor* laccase (*39*). Indeed, as a result of our protein engineering, we have succeeded in turning Fet3p into a laccase, albeit a relatively inefficient one. If we take the ET ratio, k_{HQ}/k_{Fe}, as a measure of laccase activity, this ratio goes from 0.000017 for wild-type Fet3p to 5 for the Fet3pE185A/D409A double mutant. For comparison, this ratio with HQ as the substrate for *T. versicolor* laccase, with a T1 Cu $E°$ of 434 mV also (*40*), is ~4650 (*17*).

In summary, E185, D283, and D409 play complementary roles in the trafficking of Fe from Fet3p to Ftr1p in support of high-affinity Fe uptake in yeast. With respect to the ferroxidase reaction that initiates this Fe trafficking process, their roles differ. Residue D283 contributes to the productive binding of Fe^{II} at the ET site on Fet3p and may help to tune the potential of this bound Fe^{II} for efficient electron transfer; D283 is not, however, part of the electrical wire (i.e., superexchange pathway) that connects the Fe^{II} to the T1 Cu^{II}. This role is shared by E185 and D409; through their H-bonds to the two T1 Cu ligands, H489 and H413, respectively, these two residues contribute to if not define the H_{DA} term in the Marcus equation. In addition, these two residues assist in productive Fe^{II} binding and in lowering the reduction potential of the bound Fe^{II}. We suggest that these two residues in particular, conserved in archived fungal MCO proteins known to oxidize Fe^{II} or to be required for iron homeostasis, likely define the difference between fungal and plant laccases and their ferroxidase homologues.

SUPPORTING INFORMATION AVAILABLE

^{59}Fe uptake in yeast cells expressing wild-type and mutant forms of Fet3p (Table S1) and cwEPR spectra of wild-type and mutant forms of Fet3p (Figure S1). This material is available free of charge via the Internet at http://pubs.acs.org.

REFERENCES

1. Solomon, E. I., Sundaram, U. M., and Machonkin, T. E. (1996) Multicopper oxidases and oxygenases, *Chem. Rev. 96*, 2563−2605.
2. Stoj, C. S., and Kosman, D. J. (2005) Copper Oxidases, in *Encyclopedia of Inorganic Chemistry* (King, R. B., Ed.) pp 1134−1159, John Wiley, New York.
3. Stoj, C., and Kosman, D. J. (2003) Cuprous oxidase activity of yeast Fet3p and human ceruloplasmin: Implication for function, *FEBS Lett. 554*, 422−426.
4. Kosman, D. J. (2002) Fet3p, ceruloplasmin, and the role of copper in iron metabolism, in *Advances in Protein Chemistry* (Valentine, J. S., and Gralla, E., Eds.) pp 221−269, Elsevier, New York.
5. Hellman, N. E., and Gitlin, J. D. (2002) Ceruloplasmin metabolism and function, *Annu. Rev. Nutr. 22*, 439−458.
6. Osaki, S., Johnson, D. A., and Frieden, E. (1966) The possible significance of the ferrous oxidase activity of ceruloplasmin in normal human serum, *J. Biol. Chem. 241*, 2746−2751.
7. Griffiths, T. A. M., Mauk, A. G., and MacGillivray, R. T. A. (2005) Recombinant expression and functional characterization of human hephaestin: A multicopper oxidase with ferroxidase activity, *Biochemistry 44*, 14725−14731.
8. Vulpe, C. D., Kuo, Y. M., Murphy, T. L., Cowley, L., Askwith, C., Libina, N., Gitschier, J., and Anderson, G. J. (1999) Hephaestin, a ceruloplasmin homologue implicated in intestinal iron transport, is defective in the sla mouse, *Nat. Genet. 21*, 195−199.
9. Askwith, C., Eide, D., Van Ho, A., Bernard, P. S., Li, L., Davis-Kaplan, S., Sipe, D. M., and Kaplan, J. (1994) The *FET3* gene of *S. cerevisiae* encodes a multicopper oxidase required for ferrous iron uptake, *Cell 76*, 403−410.
10. Hassett, R. F., Yuan, D. S., and Kosman, D. J. (1998) Spectral and kinetic properties of the Fet3 protein from *Saccharomyces cerevisiae*, a multinuclear copper ferroxidase enzyme, *J. Biol. Chem. 273*, 23274−23282.
11. Urbanowski, J. L., and Piper, R. C. (1999) The iron transporter Fth1p forms a complex with the Fet5 iron oxidase and resides on the vacuolar membrane, *J. Biol. Chem. 274*, 38061−38070.
12. Chidambaram, M. V., Barnes, G., and Frieden, E. (1983) Ceruloplasmin and the reactions forming diferric transferrin, *FEBS Lett. 159*, 137−140.
13. Stearman, R., Yuan, D. S., Yamaguchi-Iwai, Y., Klausner, R. D., and Dancis, A. (1996) A permease-oxidase complex involved in high-affinity iron uptake in yeast, *Science 271*, 1552−1557.
14. Quintanar, L., Gebhard, M., Wang, T. P., Kosman, D. J., and Solomon, E. I. (2004) Ferrous binding to the multicopper oxidases *Saccharomyces cerevisiae* Fet3p and human ceruloplasmin: Contributions to ferroxidase activity, *J. Am. Chem. Soc. 126*, 6579−6589.
15. Wang, T. P., Quintanar, L., Severance, S., Solomon, E. I., and Kosman, D. J. (2003) Targeted suppression of the ferroxidase and iron trafficking activities of the multicopper oxidase Fet3p from *Saccharomyces cerevisiae*, *J. Biol. Inorg. Chem. 8*, 611−620.
16. Ducros, V., Brzozowski, A. M., Wilson, K. S., Brown, S. H., Ostergaard, P., Schneider, P., Yaver, D. S., Pedersen, A. H., and Davies, G. J. (1998) Crystal structure of the type 2 Cu depleted laccase from *Coprinus cinereus* at 2.2 Å resolution, *Nat. Struct. Biol. 5*, 310−316.
17. Machonkin, T. E., Quintanar, L., Palmer, A. E., Hassett, R., Severance, S., Kosman, D. J., and Solomon, E. I. (2001) Spectroscopy and reactivity of the type 1 copper site in Fet3p from *Saccharomyces cerevisiae*: Correlation of structure with reactivity in the multicopper oxidases, *J. Am. Chem. Soc. 123*, 5507−5517.
18. Machonkin, T. E., and Solomon, E. I. (2000) The thermodynamics, kinetics, and molecular mechanism of intramolecular electron transfer in human ceruloplasmin, *J. Am. Chem. Soc. 122*, 12547−12560.
19. Taylor, A. B., Stoj, C. S., Ziegler, L., Kosman, D. J., and Hart, P. J. (2005) The copper-iron connection in biology: Structure of the metallo-oxidase Fet3p, *Proc. Natl. Acad. Sci. U.S.A. 102*, 15459−15464.
20. Singh, A., Severance, S., Kaur, N., Wiltsie, W., and Kosman, D. J. (2006) Assembly, activation and trafficking of the Fet3p, Ftr1p high affinity iron permease complex in *Saccharomyces cerevisiae*, *J. Biol. Chem. 281*, 13355−13564.
21. Bradford, M. M. (1976) A rapid and sensitive method for the quantitation of microgram quantities of protein utilizing the principle of protein-dye binding, *Anal. Biochem. 72*, 248−254.
22. Felsenfeld, G. (1960) The determination of cuprous ion in copper proteins, *Arch. Biochem. Biophys. 87*, 247−251.
23. Xu, F., Palmer, A. E., Yaver, D. S., Berka, R. M., Gambetta, G. A., Brown, S. H., and Solomon, E. I. (1999) Targeted mutations in a *Trametes villosa* laccase. Axial perturbations of the T1 copper, *J. Biol. Chem. 274*, 12372−12375.
24. Yanagisawa, S., and Dennison, C. (2005) Reduction potential tuning at a type 1 copper site does not compromise electron transfer reactivity, *J. Am. Chem. Soc. 127*, 16453−16459.
25. Palmer, A. E., Quintanar, L., Severance, S., Wang, T. P., Kosman, D. J., and Solomon, E. I. (2002) Spectroscopic characterization and O_2 reactivity of the trinuclear Cu cluster of mutants of the multicopper oxidase Fet3p, *Biochemistry 41*, 6438−6448.
26. Quintanar, L., Stoj, C., Wang, T. P., Kosman, D. J., and Solomon, E. I. (2005) Role of aspartate 94 in the decay of the peroxide intermediate in the multicopper oxidase Fet3p, *Biochemistry 44*, 6081−6091.
27. Kwok, E. Y., Severance, S., and Kosman, D. J. (2006) Evidence for iron channeling in the Fet3p-Ftr1p high-affinity iron uptake complex in the yeast plasma membrane, *Biochemistry 45*, 6317−6327.
28. Zaitseva, I., Zaitsev, V., Card, G., Moshkov, K., Bax, B., Ralph, A., and Lindley, P. (1996) The X-ray structure of human ceruloplasmin at 3.1 Å: Nature of the copper centres, *J. Biol. Inorg. Chem. 1*, 15−23.
29. Lindley, P. F., Card, G., Zaitseva, I., Zaitsev, V., Reinhammar, B., Selin-Lindgren, E., and Yoshida, K. (1997) An X-ray structural study of human ceruloplasmin in relation to ferroxidase activity, *J. Biol. Inorg. Chem. 2*, 454−463.

30. Bonaccorsi di Patti, M. C., Pascarella, S., Catalucci, D., and Calabrese, L. (1999) Homology modeling of the multicopper oxidase Fet3 gives new insights in the mechanism of iron transport in yeast, *Protein Eng. 12*, 895−897.
31. Bonaccorsi di Patti, M. C., Felice, M. R., Camuti, A. P., Lania, A., and Musci, G. (2000) The essential role of Glu-185 and Tyr-354 residues in the ferroxidase activity of *Saccharomyces cerevisiae* Fet3, *FEBS Lett. 472*, 283−286.
32. Ackers, G. K., and Smith, F. R. (1985) Effects of site-specific amino acid modification on protein interactions and biological function, *Annu. Rev. Biochem. 54*, 597−629.
33. Wells, J. A. (1990) Additivity of mutational effects in proteins, *Biochemistry 29*, 8509−8517.
34. Marcus, R. A., and Sutin, N. (1985) Electron transfer in chemistry and biology, *Biochim. Biophys. Acta 811*, 265−322.
35. DeBeer George, S., Basumallick, L., Szilagyi, R. K., Randall, D. W., Hill, M. G., Nersissian, A. M., Valentine, J. S., Hedman, B., Hodgson, K. O., and Solomon, E. I. (2003) Spectroscopic investigation of stellacyanin mutants: Axial ligand interactions at the blue copper site, *J. Am. Chem. Soc. 125*, 11314−11328.
36. Olsson, M. H., Ryde, U., and Roos, B. O. (1998) Quantum chemical calculations of the reorganization energy of blue-copper proteins, *Protein Sci. 7*, 2659−2668.
37. Betts, J. N., Beratan, D. N., and Onuchic, J. N. (1992) Mapping electron tunneling pathways: An algorithm that finds the "minimum length"/maximum coupling pathway between electron donors and acceptors in proteins, *J. Am. Chem. Soc. 114*, 4063−4046.
38. Roberts, S. A., Wildner, G. F., Grass, G., Weichsel, A., Ambrus, A., Rensing, C., and Montfort, W. R. (2003) A labile regulatory copper ion lies near the T1 copper site in the multicopper oxidase CueO, *J. Biol. Chem. 278*, 31958−31963.
39. Bertrand, T., Jolivalt, C., Briozzo, P., Caminade, E., Joly, N., Madzak, C., and Mougin, C. (2002) Crystal structure of a four-copper laccase complexed with an arylamine: Insights into substrate recognition and correlation with kinetics, *Biochemistry 41*, 7325−7333.
40. Reinhammar, B. R. (1972) Oxidation-reduction potentials of the electron acceptors in laccases and stellacyanin, *Biochim. Biophys. Acta 275*, 245−259.

BI061543+